Applied Catalysis B: Environmental 330 (2023) 122589

Contents lists available at ScienceDirect

Applied Catalysis B: Environmental

journal homepage: www.elsevier.com/locate/apcatb

Tuning flow-through cu-based hollow fiber gas-diffusion electrode for high-efficiency carbon monoxide (CO) electroreduction to C_{2+}products

Hesamoddin Rabiee [a,b,c], James K. Heffernan [d], Lei Ge [b,c,*], Xueqin Zhang [a], Penghui Yan [c], Esteban Marcellin [d], Shihu Hu [a,**], Zhonghua Zhu [c], Hao Wang [b], Zhiguo Yuan [a]

[a] Australian Centre for Water and Environmental Biotechnology (ACWEB), The University of Queensland, St. Lucia, Queensland 4072, Australia
[b] Centre for Future Materials, University of Southern Queensland, Springfield, QLD 4300, Australia
[c] School of Chemical Engineering, The University of Queensland, Brisbane, QLD 4072, Australia
[d] Australian Institute for Bioengineering and Nanotechnology, The University of Queensland, 4072 QLD, Australia

ARTICLE INFO

Keywords:
Electrochemical carbon monoxide reduction
Flow-through gas-diffusion electrode
Hollow fiber
Ethylene production

ABSTRACT

Electrochemical carbon monoxide reduction (CORR) to C_{2+} products has advantages over electrochemical CO_2 conversion (CO_2RR) as issues such as carbonation, and CO_2 loss during CO_2RR are omitted in CORR due to the stability of CO in alkaline solutions. Facing common challenges as CO_2RR, CORR suffers more from mass transport resistance and intrinsically lower aqueous CO solubility. Therefore gas-diffusion electrodes (GDEs) are desired to boost the formation of triple phases and active sites to obtain higher reaction rates. Herein, for the first time Cu-based hollow fiber GDEs (HFGDEs) are tuned for CORR to C_{2+} products. By growing a layer of Cu nanocubes as the catalyst layer on HFGDEs, non-selective pristine copper HFGDE became highly selective for C_{2+} products (FE>90%), with ethylene as the main product (FE>65%), owing to the dominant Cu (100) facet in Cu nanocubes with high C_{2+} selectivity. In addition, ultra-high ethylene partial current density of > 470 mA cm^{-2} at − 0.8 V vs. RHE in 5.0 M KOH was obtained, owing to the abundant porosity and surface area available for triple-phase formation on microtubular GDEs and their enhanced mass transport. The electrodes exhibited one of the highest partial current densities achieved for ethylene production, indicating the promises of flow-through hollow fiber configuration for other desired products or gas-phase electrochemical reactions with low aqueous solubility.

1. Introduction

The conversion of carbon dioxide (CO_2) or carbon monoxide (CO) to commodity fuels and chemicals, empowered by low-carbon electricity, has attracted much attention as an alternative to conventional routes of chemical production [1]. Numerous studies have focused on CO_2 reduction to CO or formic acid and active/efficient electrocatalysts with high Faradaic efficiencies (FEs) have been developed [2,3]. However, CO_2 reduction to higher value C_{2+} products needs the critical C-C coupling step, and to date, Cu has been the main electrocatalyst for this conversion [4]. Despite the high activity, Cu is an intrinsically non-selective electrocatalyst for CO_2RR, and achieving high FE for C_{2+} products is challenging [5,6]. A two-step conversion ($CO_2 \rightarrow CO \rightarrow C_{2+}$ products) has several advantages over the direct CO_2 electrolysis to C_{2+} products. During CO-to-C_{2+} conversion, formic acid and/or CO, which compete with C_{2+} production during CO_2RR, are not produced [7]. In addition, CO has inherent stability in alkaline solutions, whereas CO_2RR suffers from carbonation (as a result of CO_2 reaction with alkaline electrolyte) which adversely affects the stability of CO_2RR [8]. Also the crossover of CO_2 to the anode side in the form of carbonate results in CO_2 loss [9]. These advantages have made CORR a promising option for C_{2+} production following CO_2 reduction to CO. Cu-based electrocatalysts have been developed recently for selective CORR to several C_{2+} products [10,11]. In particular, Cu-based electrocatalysts with lattice facet [100] have been shown to facilitate C-C coupling for C_{2+} production [12,13]. The cubic shape Cu nanoparticles are dominantly made of this specific lattice facet and high selectivity towards ethylene has been reported on Cu nanocubes [13,14].

CO has a low aqueous solubility, even lower than that of CO_2, which hinders obtaining conversion near industrially relevant rates. To deal

* Corresponding author at: Centre for Future Materials, University of Southern Queensland, Springfield, QLD 4300, Australia.
** Corresponding author.
E-mail addresses: lei.ge@usq.edu.au (L. Ge), s.hu@awmc.uq.edu.au (S. Hu).

https://doi.org/10.1016/j.apcatb.2023.122589
Received 25 October 2022; Received in revised form 2 February 2023; Accepted 5 March 2023
Available online 8 March 2023

with this issue, gas-diffusion electrodes (GDEs) are utilized to feed the gaseous reactant near the catalyst surface, increasing the gas concentration and shortening the diffusional path [15–17]. Conventional planar GDEs consist of several layers, but are often complicated for mass production and suffer from flooding of the electrolyte to the gas side [8]. While GDEs have been used for CO_2RR widely in recent years [18,19], their use for CORR needs more exploration.

Hollow fiber GDEs (HFGDEs), a new electrode configuration as an alternative to planar GDEs, have been studied for CO_2RR with promising results, owing to their unique tubular shape, abundant catalytic active sites, and ease of production [20–22]. Despite some encouraging results, HFGDEs have not outperformed planar GDEs, when used in CO_2RR using alkaline electrolytes, in terms of the current density [23]. The gas delivery configuration of HFGDEs is flow-through [24], meaning that the gas is in full contact with the electrolyte on the outer layer of HFGDEs [25]. This limits the application of HFGDEs for CO_2RR. Therefore, using HFGDEs for CO_2RR is limited to using non-alkaline electrolytes (e.g., $KHCO_3$) due to the interaction between CO_2 and OH^- in flow-through mode. However, this limitation is not expected for CORR, due to the mentioned stability of CO in alkaline media. When used in alkaline electrolytes, HFGDEs are expected to achieve high current densities for CORR. Moreover, during CO_2RR in alkaline/neutral electrolytes, CO_2 can cross-over to the anion side in the form of HCO_3^-/CO_3^{2-} ions, leading to CO_2 loss during the reaction and unfavorable carbon loss [26]. This is even more serious for HFGDEs since CO_2 dissolves in the electrolyte in the flow-through mode, but it is not expected to be a problem for CO during CORR.

Herein for the first time we design Cu-based HFGDEs for efficient CORR to C_{2+} products with ethylene as the main product. The pristine Cu HFGDEs showed low selectivity towards C_{2+} products. Therefore, we tuned the Cu catalyst shape morphology and orientated growth of nanocubes on the outer surface of HFGDEs by electrodeposition. Due to the efficient C-C coupling and high C_{2+}selectivity of copper nanocubes with dominant Cu (100), the HFGDEs showed exceptionally high current densities in the 1.0 M KOH electrolyte, outperforming conventional GDEs tested for CORR under similar conditions. Compared with CO_2RR in a bicarbonate medium, significantly higher current densities and FEs of C_{2+} products (>90%) and ethylene (>65%) were achieved when the HFGDE were used for CORR. Moreover, lower partial current densities of C_{2+} were obtained when using the hollow fibers in the non-GDE mode, confirming the significant performance of HFGDEs for achieving high-rate and selective CO reduction through maximizing triple-phase interfaces and local CO concentration. By increasing the concentration of KOH, an ethylene partial current density of 472 mA cm^{2-} was obtained using the flow-cell reactor, indicating the promises of HFGDEs as an emerging electrode configuration for efficient CORR to C_{2+} products.

2. Experimental

2.1. Fabrication and characterization of Cu-based hollow fibers

The pristine Cu hollow fibers were fabricated through a two-step phase inversion and thermal treatment process [20] (Fig. S1). In brief, copper particles (65 wt%, 5–10 μm, 99%, Sandvik, UK) were added to the polymer solution (8.75 wt% Polyethersulfone 6020 P, BASF, Germany in 26.25 wt% solvent (N-methyl-2-pyrrolidone)). The dope was extruded into a spinneret rig (outer diameter of 1.9 mm, inner diameter of 0.7 mm) to the water bath as the non-solvent. This leads to phase separation of the solvent and the non-solvent, and polymeric solution solidifies into a microtubular shape and is stored overnight in the water to remove the solvent completely. The polymer was burnt away at 600 °C using a tubular furnace (air atmosphere, 2 h) and this leads to oxidation of Cu which were reduced back to Cu at 500 °C in H_2/Ar (10%/90%) for 1 h. To prepare CuCube HFGDEs, cubic shape Cu particles were electrodeposited on the outer side of the Cu HFGDE [27]. The pristine Cu HFGDEs were first electropolished in 85 wt% phosphoric acid at 3.0 V vs stainless steel mesh for 5 min. Electrodeposition of Cu nanocubes was done using a mixture of 50 mM copper sulfate-pentahydrate ($CuSO_4 0.5\ H_2O$) and 50 mM potassium chloride (KCl) as the electrodeposition bath via cycling between a reducing potential (+0.22 V vs. RHE) and an oxidizing (+0.55 V vs. RHE). The cycling continued until the outer surface of Cu HFGDE was uniformly covered by copper nanocubes. During the electrodeposition, HFGDE was purged by Ar to ensure the surface pores are not blocked. All materials are purchased from Sigma unless otherwise specified. A Hitachi HF5000 (accelerating voltage of 200 kV) was used to acquire high-resolution transmission electron microscopy (HRTEM) images. For HRTEM, the outer layer of CuCube HFGDE was scratched lightly to collect some electrodeposited copper cubes. A JOEL-7100 F (equipped with an energy dispersive X-ray analyzer (EDX)) was used to achieve field emission scanning microscopy (FESEM) images. X-ray diffraction (XRD) was obtained on a Rigaku SmartLab (Cu Kα (λ = 1.5405 Å) radiation source). Agilent 7900 Quadrupole Inductively Coupled Plasma Mass-Spectrometer (ICP-MS) was used to detect copper in the electrolyte after reaction. The electrolyte was diluted by 20 times with 2% double-distilled HNO_3 for ICP-MS.

2.2. CO electroreduction and analysis of products

CORR experiments were carried out in a 3-electrode reactor. Catholyte/anolyte (170 ml) were used in two compartments, separated by Fumasep FAB-PK-130 anion exchange membrane (Fuel Cell store, USA). Hollow fibers (4.5–5 cm, outer diameter of around 1.3–1.5 mm measured via a digital micrometer) were used as the working electrode (cathode), immersed in the catholyte (Fig. S2). A Pt wire was the counter electrode (anode) for the anodic water splitting. As the reference electrode, an Hg/HgO (1 M NaOH, Bioanalytical Systems, USA) was placed near the HFGDE. The electrolyte was 1.0 M KOH, unless stated otherwise. One end of HFGDEs was sealed with epoxy and CO (99.9%, Coregas, Australia) was fed from the other end (Fig. S2). A mass flow controller controlled gas flow rate (20 ml min^{-1}) (*Bronkhorst,* Netherlands, ± 1% resolution). A Hg/HgO reference electrode was used to set the potential and the potentials were converted to reversible hydrogen electrode (RHE) scale via E (V vs. RHE) = E (V vs. Hg/HgO) + $E^o_{Hg/HgO}$ + 0.0591 $pH_{catholyte}$, $E^o_{Hg/HgO}$ is 0.14 for the Hg/HgO reference electrode filled with 1 M NaOH solution. A Metrohm LL Unitrode PT1000 probe measured the pH of the catholyte. Electrochemical tests (e.g., linear scanning voltammetry (LSV), chronoamperometry, and cyclic voltammetry (CV)) were done by a BioLogic SP-200 potentiostat. The current density was calculated based on the outer surface area of the hollow fiber electrodes considering their length and outer diameter. The electrodes were conditioned by CV scans between − 1.2 and − 1.6 V vs. Hg/HgO (100 mV s^{-1}), followed by 30 min pre-reduction at − 1.6 V vs. Hg/HgO under CO purging until a stable current was recorded. To estimate the electrochemically active surface area of the electrodes via the dual-layer capacitance (C_{dl}), CVs over a 0.1 V window near the open-circuit voltage at scan rates from 20 to 100 mV s^{-1}, followed by:

$$C_{dl} = J \Big/ \left(\frac{dV}{dt}\right) \quad (1)$$

where J is the current density in the center of 0.1 V window, and $\frac{dV}{dt}$ is the CV scan rate. CO was purged through the HFGDEs while conducting CV scans to obtain C_{dl}.

Linear scanning voltammetries were obtained from − 0.2 V to − 1 V vs. RHE with the sweeping rate of 5 mV s^{-1} in CO/Ar-saturated electrolyte after 20 min of gas fed through HFGDEs. To obtain the faradaic efficiency (FE) of products at various potentials, chronoamperometry was done under CO purging through the HFGDEs for 1 h between − 0.4 and − 1.0 V vs. RHE. After 30 min of applying potential and reaching the steady-state condition, gas and liquid samplings were done.

Liquid products were measure with high-performance liquid chromatography (HPLC) (Shimadzu, Hi-Plex H, 7.7 ×300 mm, 8 μm column, SPD-20A/20AV UV-Vis detector). The FE of liquid products were calculated using the following equation:

$$FE_i = \frac{e_i \times F \times n}{Q} \quad (2)$$

where e_i is the electron transfer for the production of liquid production from CO (8 for ethanol, 12 for propanol and acetate), F is Faraday's constant (96485 C mol^{-1}), and n is the moles of the produced liquid product measured via HPLC. Q represents the total charge during the experiment (calculated by the measured current and sampling time).

An online Hiden HPR-20-QIC mass spectrometer analyzed gaseous products. In the reactor off-gas, the detector monitored the intensities of H_2, CO, methane, and ethylene at 2, 12, 15, and 27 at. mass units (amu). The FE of gaseous products was determined via the following equation:

$$FE_i = \frac{e_i \times F \times P \times V \times X_i}{J \times R \times T} \times 100 \quad (3)$$

where e_i is the electron transfer required (in mole) to generate one mole of a gas product (2 for H_2, 6 for methane, and 8 for ethylene), X_i represents the products concentration in the reactor gas outlet measured with the mass spectrometer, V is the outlet gas volumetric flow rate (ml min^{-1}), P is the atmospheric pressure (101.3 kPa), and J is the current (mA) (from the potentiostat).

For the stability experiment (for 36 h), the HFGDEs were tested in a custom-built flow cell (Fig. S3) and electrolytes in the anodic/cathodic sections (each 20 ml) were circulated (10 ml min^{-1}) with peristaltic pumps. Two reservoir containers (volume of 2 L) were used for catholyte/anolyte, and CO was purged through the hollow fibers (20 ml min^{-1}) throughout the test. A bundle of HFGDEs (three fibers in this study, Fig. S3) can be used in the flow-cell reactor. The outlet flow of

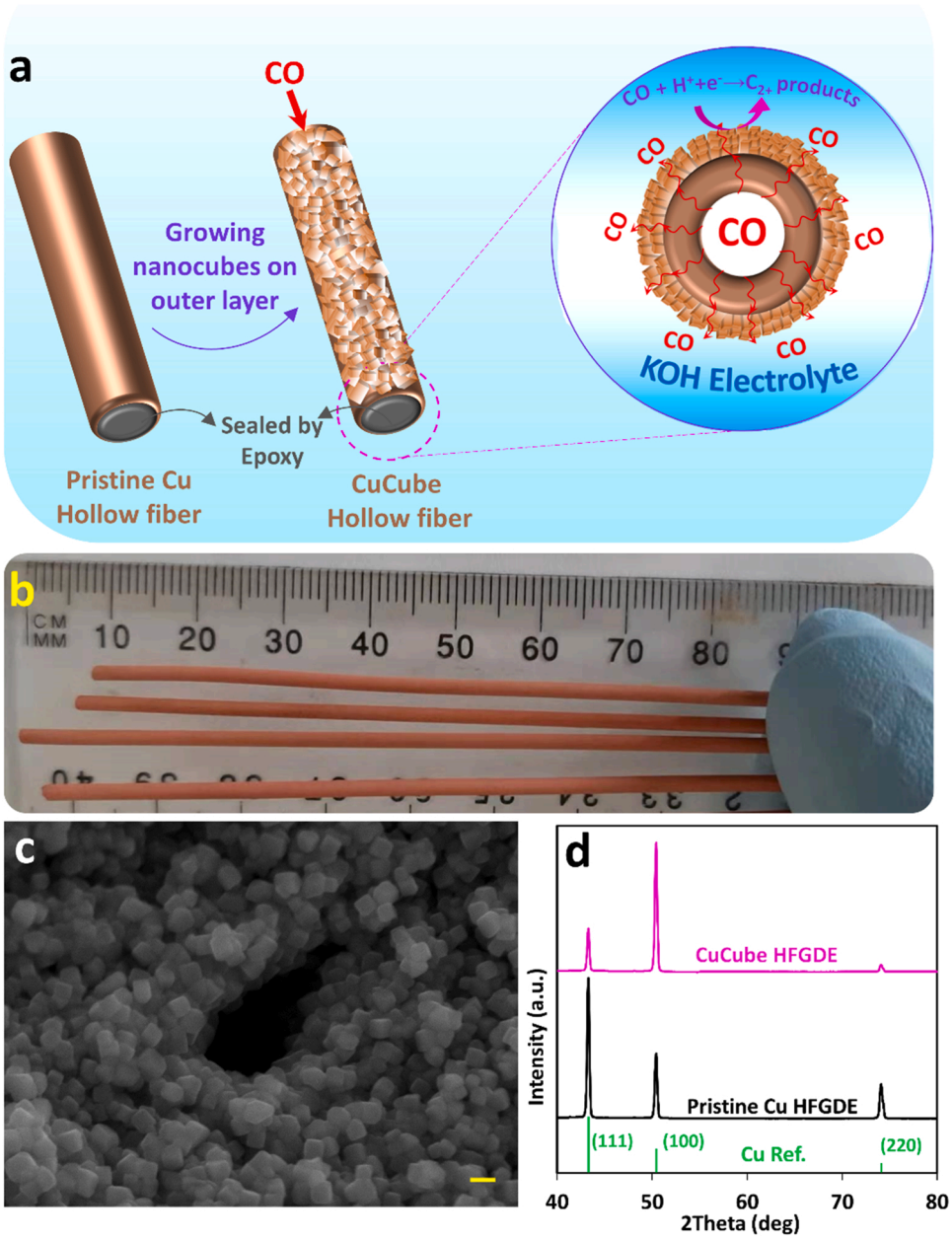

Fig. 1. a) Schematic of hollow fiber GDEs and growing nanocubes on the outer layer for CO reduction reaction in KOH electrolyte; b) Image of a bundle Cu hollow fibers handheld; c) FESEM image of CuCube HFGDE with nanocubes covering the surface in size around 50 nm (scale bar: 50 nm); d) XRD of pristine and CuCube HFGDEs.

the reactor was connected to a cold trap bottle to separate gas (including unreacted CO and gas products) from the electrolyte. Samplings of liquid and gas were done each hour. The average value of three tests is reported for each electrochemical test.

3. Results and discussion

3.1. Characterization and structure of Cu-based HFGDEs

The schematic of using Cu-based HFGDEs for CORR is shown in Fig. 1a. Cu HFGDEs were fabricated through dry-wet process, the method used in our previous works (schematically shown in Fig. S1) [25]. Hollow fibers made of Cu with a uniform wall thickness of 150 μm (Fig. S4) and a diameter of 1.3–1.5 mm are shown Fig. 1b. A sharp energy dispersive X-ray (EDX) peaks of copper was observed for Cu HFGDE (Fig. S5), indicating the complete removal of polymer. Moreover, high electrical conductivity was measured for the fibers (Table S1), resulting from the tight sintering of Cu particles together. The surface of Cu HFGDEs exhibited metallic luster with abundant micrometer-sized pores on the outer surface of the fibers (Fig. S4b). The Cu hollow fibers comprised well-connected Cu particles (Fig. S4) as a result of sintering with surface pores for CO delivery to the outer surface where the reaction takes place. To reach the gas flow rate of 20 ml min^{-1} for the fabricated hollow fibers, an overpressure of 0.5–0.7 atm was required,

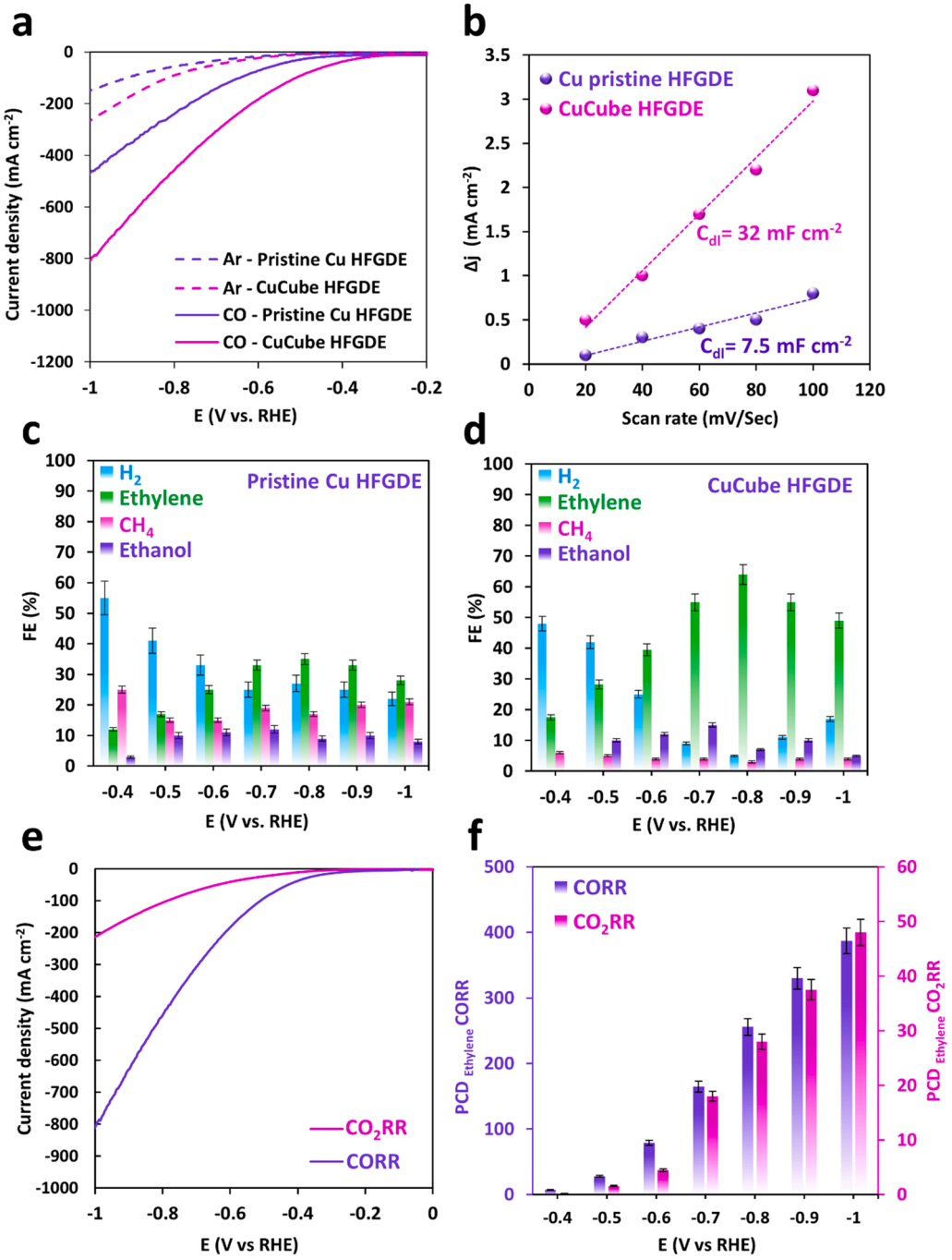

Fig. 2. a) Linear sweep voltammetry of pristine Cu and CuCube HFGDEs with CO and Ar purging through; b) Dual-layer capacitance (Cdl) of pristine Cu and CuCube HFGDEs; FE of major products (H_2, ethylene, methane, and ethanol) for c) pristine Cu and d) CuCube HFGDEs; e) Linear sweep voltammetry of CuCube HFGDE for CORR and CO_2RR; f) Partial current density of ethylene obtained from CORR and CO_2RR.

providing CO permeability of $4.3 \pm 0.5 \times 10^{+6}$ Barrer (calculated via Eq. S1).

The formation of Cu nanocubes on the outer surface of Cu HFGDEs can be seen in Fig. 1c, where Cu nanocubes with the size of around 50 nm uniformly cover Cu HFGDE. Increasing the numbers of CV cycles results in more coverage of the Cu HFGDE by nanocubes (Fig. S6) and after 30 cycles the outer layer of Cu HFGDE is uniformly covered by Cu nanocubes, as seen in Fig. 1c and cross-sectional images (Fig. S7). CO permeability of the hollow fibers remained in the same range ($4.3 \pm 0.5 \times 10^{+6}$ Barrer), confirming that the surface pores are not blocked during electrodeposition. The X-ray diffraction (XRD) analysis of the Cu and CuCube HFGDEs (Fig. 1d) confirmed the increase in the strength of Cu (100) as a result of having nanocubes on the outer layer, and much weaker peaks related to Cu (111) and Cu (220) as a result of the covering Cu nanocube layer. The existence of Cu (111) and Cu (220) after coverage with Cu nanocubes can be attributed to either the Cu substrate which is picked up during XRD analysis or the electrodeposited Cu layer as electrodeposited copper is not exclusively in cubic shape. However, from the FESEM images (Fig. 1c, S6) and XRD results (Fig. 1d), it can be concluded that copper cubes are the dominant shape of the electrodeposited layer. In addition, the high-resolution TEM image of the electrodeposited copper cubes showed the crystalline structure of the electrodeposited Cu layer and the existence of lattice strips with a d-spacing of 0.18 nm which is associated with Cu (100) (Fig. S8).

3.2. Electrocatalytic CORR performance

The HFGDEs were tested for CORR to determine their efficiency for CO conversion. The electrochemical activity of Cu-based HFGDEs for CORR assessed via LSV (5 mV s^{-1} scan rate). It showed a trend of very low current density at potentials more positive than − 0.3 V vs. RHE and increase at more negative potentials where CORR and H_2 evolution from water splitting occur simultaneously (Fig. 2a). The HFGDE coated with nanocube Cu particles showed a higher current density than the pristine Cu HFGDE. This is due to nanocube particles with corner and grain boundaries between them, leading to higher electroactive surface areas. This was further confirmed by measuring the electrochemical surface area (ECSA) of the HFGDEs. The dual-layer capacitance of the HFGDEs (C_{dl}) calculated from the CV cycles at various scan rates (Fig. S9) demonstrated a noticeably higher ECSA for CuCube HFGDE as compared with the pristine Cu HFGDE, as seen in Fig. 2b. This verifies more active sites of CuCube HFGDE due to the increase in the electrode roughness with abundant sharp edges and corners of nanocubes. Moreover, the current densities obtained when Ar is purged through the HFGDEs were significantly lower than when CO was used, as seen in Fig. 2a, indicating the high activity of the HFGDEs for CORR. The current with Ar purging comes from the water splitting half-reaction, however when CO is purged CORR competes with H_2 evolution. It was also observed that increasing the CO flow rate up to 20 ml min^{-1} led to a higher current density, and after that, the current density did not change significantly with the CO flow rate (Fig. S10). This implies that most active sites are involved in the gas-phase CORR at this flow rate, and the catalyst has reached its intrinsic limit [21].

The gaseous outlet was analysed to determine the CORR product selectivity of Cu-based HFGDEs. A significant increase in the FE of ethylene was seen for CuCube HFGDE, reaching 65% (>90% for C_{2+} products) at − 0.8 V vs. RHE. In comparison, with the pristine Cu HFGDE, FE of ethylene did not exceed 34%. This comes from the existence of Cu nanocubes with dominant Cu (100) steps which is efficient for CO_2RR and CORR to C_{2+} products, particularly ethylene formation [27–30]. In addition to ethylene, methane and H_2 (from half-reaction water splitting) are the other gaseous products detected during CORR. High ethylene FE for CuCube HFGDE was associated with lower FE of methane and H_2 compared to the pristine Cu HFGDE (Fig. S11). As can be seen in Fig. 2c & d, the FE of methane for CuCube HFGDE is less than 5% compared to as much as 20% for pristine Cu HFGDE. This difference comes from the formation/suppression of key intermediates on these two electrodes with different crystalline structures. The formation of C_{2+} products and methane during CORR occurs on distinct types of active sites through different pathways [31]. The experiments supported by density functional theory calculations by Schouten et al. [32,33], Peterson et al. [34], and Durand et al. [35] showed that hydrogenation of CO to form CHO_{ads} is the key step for the formation of both methane and ethylene on Cu electrodes. An alternative pathway of ethylene formation, suggested by Schouten et al., is via the formation of a CO dimer (C-C bond formation as a result of two CO molecules dimerization) [32]. Since this CO dimerization is most efficient on Cu (100) lattice, ethylene production is boosted on CuCube HFGDEs with stronger Cu (100) lattice. Meanwhile, methane formation occurs through CO hydrogenation. Density functional theory calculations have shown that Cu (100) has a lower activation barrier than Cu (111), favoring suppression of CO hydrogenation and therefore methane formation [36]. Consequently, a lower FE of methane is observed for CuCube HFGDEs. Thus, the cubic shape of CuCube HFGDEs is responsible for favouring ethylene formation and suppressing CO hydrogenation [13].

In addition to the gaseous products, liquid products including ethanol, acetate, and n-propanol were also detected via HPLC. The FE of liquid products was much lower than that of ethylene. Within the tested potential range, acetate production was minor, with an FE less than 5%. FE of ethanol fluctuated between 4% and 14% for both pristine and CuCube HFGDEs. The maximum n-propanol FE of 18% was observed for CuCube HFGDE at − 0.8 V vs. RHE (Fig. S12), where ethylene FE was also maximized. This is a result of high ethylene FE, which leads to a higher local concentration of C_2H_4(ads) – a necessary intermediate for n-propanol production [37,38].

To further examine the efficiency of CuCube HFGDE for the formation of C_{2+} products, CORR was compared to CO_2RR. For CO_2RR on pristine Cu HFGDE, C_1 products (mainly CO and formate) were the dominant ones, with the FE of ethylene being lower than 16% within the tested potential range (Fig. S13) [20,39]. By performing CO_2RR on CuCube HFGDE, an increase in the FE of C_{2+} products was observed (up to 28% ethylene FE) since cubic Cu favors the formation of C_{2+} products in general [27–30]. However, FE of C_{2+} products, and in particular ethylene, is much lower than observed in CORR. The maximum FE for C_{2+} products was 36% for CuCube HFGDE during CO_2RR, compared to > 90% for CORR. Other products such as ethanol and n-propanol were minor (up to 6% each). The FE of H_2 on CuCube was fairly less than that of pristine Cu HFGDE (Fig. S13), which is consistent with results in the literature for CO_2RR on Cu electrode [12]. The trend of FE observed for different products from CO_2RR and CORR confirms a higher suitability of CORR for C_{2+} formation over CO_2RR [7]. The main reasons are: 1) During CORR the high local CO concentration makes C-C coupling easier, where CO dimerization is necessary for C-C coupling and C_{2+} formation, 2) The competing reaction to formate does not exist during CORR, and 3) For a specific product, less electron transfer is required during CORR (e.g., ethylene production requires $8e^-$ from CO, but 12 e^- from CO_2).

Comparison of the current densities for CORR and CO_2RR gives us a clearer view of CORR's enhanced efficiency over CO_2RR. The obtained current density with CORR is 3–5 times higher than CO_2RR (Fig. 2e), resulting in a much higher partial current density (PCD) of C_{2+} formation from CORR, as can be seen in Fig. 2f. This could be due to performing CORR in KOH as compared to CO_2RR in $KHCO_3$ electrolyte. Alkaline electrolytes (KOH) have higher ionic conductivity than $KHCO_3$ and in this study cell resistance measured to be ~ 8.5 and 4.8 Ω with 1 M $KHCO_3$ and 1 M KOH, respectively (electrochemical impedance spectroscopy results in Fig. S14) [15,40]. Moreover, Parasitic H_2 evolution is suppressed in alkaline electrolytes [23], and we generally observed a lower FE of H_2 for CORR in KOH compared to CO_2RR in $KHCO_3$. The simultaneous achievement of a higher FE for C_{2+} products and a higher current density from CORR led to a much-improved performance. It should be noted that CO_2RR with HFGDEs cannot be performed in

alkaline media. The gas delivery mechanism of HFGDEs is flow-through, and due to the direct reaction between CO_2 and OH^- alkaline electrolyte, cannot be used in this electrode configuration. The mechanism of gas delivery in HFGDEs is further discussed in the following section.

3.3. The mechanism of CO delivery in HFGDEs

Hollow fiber GDEs used for CORR demonstrated much higher current density than other electrodes simply immersed into the electrolyte in the literature [41,42] and a better performance than most of the state-of-art conventional planar GDEs used for CORR [43–45]. To further investigate the efficiency of CO delivery by HFGDEs, we tested CuCube HFGDE for CO reduction in non-GDE mode, where one end of HFGDE is not blocked and CO travels through the inner side of the HFGDE, as shown in Fig. 3a. Unlike the GDE mode, gas pressure does not build up inside the HFGDE and CO flows out the end of the HFGDE. The performance of the same electrode in GDE and non-GDE modes shows much higher electrocatalytic activity is observed in GDE mode. The GDE mode creates turbulence and encourages interactions between CO active sites on the outside surface of the HFGDE as CO is pushed through the wall. This guarantees a sufficient supply of CO to the catalyst layer, leading to improved triple-phase interface formation and optimized kinetics for CORR consequently [24,46].

The gas delivery configuration of HFGDEs is flow-through, meaning a pressure differential pushes the gas-side feed, through the diffusible HF wall to the electrolyte-side [22]. This contrasts with conventional planar GDEs where the mechanism is flow-by, and the gaseous feeds do not dissolve in the electrolyte. With the flow-through configuration, the concentration gradient is diminished, leading to enhanced gas supply to the active catalyst layer, especially for high current densities that a sufficient CO supply is critical [24,25,46]. Li et al. recently reported unprecedentedly high current density of CO_2 reduction to CO on silver hollow fibers [47], indicating the potential of HFGDEs and flow-through designs for enhancing triple-phase interface formation on the catalyst layer and achieving high current densities. A high flow rate of the CO feed, rushing into the catalyst layer in the flow-through mode of HFGDEs, maintains a high local CO concentration near the triple-phase interface sites. This causes CORR to dominate in GDE mode rather than

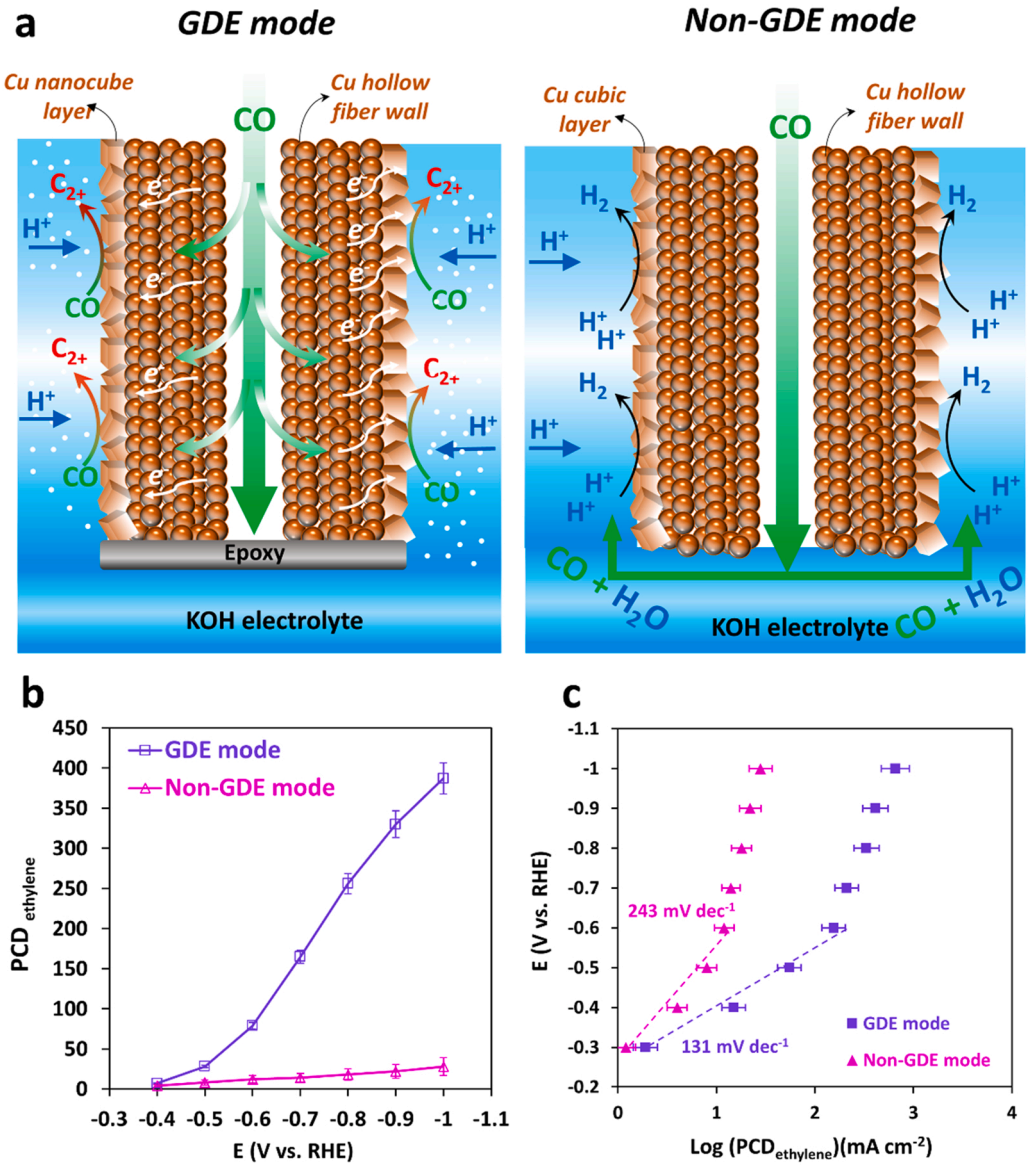

Fig. 3. a) Schematic of CO delivery mechanism in GDE and non-GDE mode, in GDE mode the HFGDEs are dead-end therefore CO diffuses through the hollow fiber walls under pressure; b) partial current density (PCD) of ethylene formation on CuCube HFGDE as a function of the applied potential in GDE and non-GDE mode; c) Tafel slopes of CuCube HFGDE in GDE and non-GDE modes.

the H_2 evolution reaction, which is prevalent in non-GDE mode due to abundant H^+ presence and insufficient CO supply from the bulk electrolyte [47,48]. As shown in Fig. 3b, the partial current density of ethylene production in the non-GDE mode is nearly 10 times lower than that for GDE mode, confirming that many available catalytic sites are not active in the non-GDE mode. In addition, pushing CO through the GDE leads to the desorption and transport of ethylene away from the reactive sites, therefore avoiding the blockage of catalytic active sites for the continuous formation of the triple-phase CO-electrolyte-catalyst interface [46].

To explore the kinetic of CORR in GDE and non-GDE, Tafel slopes (the overpotential versus log($PCD_{Ethylene}$)) in both modes were compared. It should be noted that Tafel slopes are often calculated in low overpotentials (low current densities) as at higher current densities larger amount of gas production may cause voltage fluctuations [49,50]. As can be seen in Fig. 3c, the Tafel slope for non-GDE mode is 243 mV.dec^{-1}, and is 131 mV.dec^{-1} for the GDE mode. The latter is close to the theoretical Tafel value of 118 for CORR to ethylene when the rate-determining step is the initial one-electron transfer, as reported in the literature [31,49,51]. The higher Tafel slope for non-GDE mode implies a higher catalytic activity and more efficient mass transport of CO to the catalytic active sites in GDE mode. In addition, the Tafel slope at high-overpotential for GDE-mode is lower than non-GDE mode, suggesting that non-GDE mode is likely to be limited by CO mass transfer [47]. These results indicated that the improved triple-phase interface formation and mass transfer via GDE mode of HFGDEs enhances the intrinsic CO reduction activity, leading to a higher activity and selectivity for CO reduction to ethylene.

3.4. Effects of local environment and pH

We further explored the effect of electrolyte type/concentration on the CORR performance to understand the effect of local environment conditions. CORR was completed in 1.0 M $KHCO_3$ and various concentrations of KOH (0.5, 1, 2 and 5 M), as the most common electrolyte used for CORR in literature. Having a higher concentration of KOH leads to a higher OH^- concentration and an elevated local pH in the vicinity of HFGDE during CO reduction [52] and the KOH concentrations here have a higher pH than $KHCO_3$. The higher pH of KOH is known to shift the product distribution of both CO_2RR and CORR towards C_{2+} products [38,53]. CORR current densities were greater in KOH than $KHCO_3$, and increased with concentrations of KOH (Fig. 4a). The increase in the current density was particularly noticeable when increasing KOH concentration over 0.5 KOH, then to a lesser extent from 1 M to 2 M and 5 M (Fig. S15). This is attributable to the reduction in charge transfer resistance across the electrolyte, due to increasing electrolyte conductivity with KOH concentration and subsequent improvements to the active area of the triple-phase boundary [44,54]. For the product selectivity, a higher FE for H_2 evolution was observed in $KHCO_3$, likely due to bicarbonate which acts as the proton donor, contributing to more H_2 generation and a lower FE of ethylene [55,56]. Therefore, as shown in Fig. 4a, the synergy of higher current density and ethylene FE, results in higher partial current density of ethylene with KOH as the electrolyte. In addition, Increasing the KOH concentration from 1 M to 5 M led to the reduction of both cell resistance and charge transfer resistances (Fig. S14), attributing to the higher current density obtained in 5 M KOH electrolyte.

The higher pH at the interface favors C-C coupling through

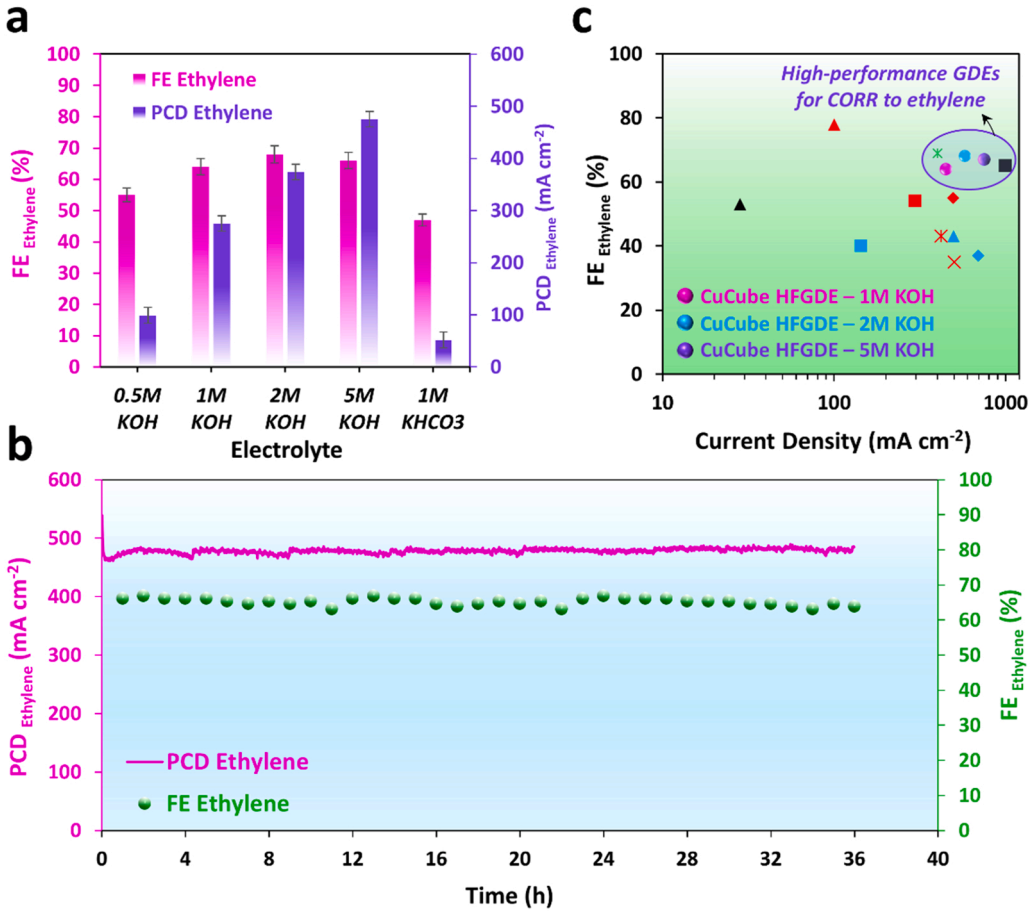

Fig. 4. FE and PCD of ethylene with different electrolytes; b) long-term operation of the HFGDE-based flow-cell with CuCube for CORR in 5 M KOH; c) Comparison of FE and total current density of CORR to ethylene in this study with the recently reported values (more details about the studies can be found in Table S3).

dimerization of adsorbed CO, suppressing the C_1 pathways by kinetics, and consequently facilitates the formation of multi-carbon products [44]. This is also consistent with the computational analysis done by Xiao et al. [57] showing that at a high pH, C-C coupling through adsorbed CO dimerization dominates, suppressing the C_1 pathways. The total FE of C_{2+} products increased slightly with KOH concentration (from 88% for 1 M KOH to 92% for 5 M KOH), indicating that the local pH slightly affects the total product selectivity. However, a slight increase in acetate formation was observed at higher concentrations of KOH, along with a decline in ethanol/propanol formation and a minor increase for ethylene FE (64–68%) (Fig. S16), consistent with the literature [43,51]. The increase in the FE of acetate can be attributed to the fact that OH^- is able to catalyze ketene ($O{=}C{=}CH_2$) to generate acetate [58]. Ma et al. [52] recently reported that changing the electrolyte solution in CORR resulted in a different local pH (in the vicinity of the electrode), while the surface pH (on the electrode surface) was almost identical. This is consistent with the theory behind acetate formation via solution reaction as the key step, which is predominantly affected by the local pH value close to the electrode surface.

The effect of cation (K^+) concentration is also important for the electrolyte concentrations. It has been shown that increasing the K^+ concentration leads to a higher C_{2+} selectivity [38], attributed to double layer saturation with cation concentrated near the electrode surface at high bulk cation concentrations [59]. This effect is more significant at a relatively low concentrations of K^+ (e.g., below 0.3 M), while in this study, the lowest KOH concentration is 0.5 M. In addition, the difference between the product selectivities for 1.0 M KOH and 1.0 $KHCO_3$, with the same K^+ concentration, can confirm the effect of local pH rather than that of the cation concentration. Moreover, a higher concentration of K^+ ions in the outer Helmholtz plane (OHP) of the electrical double layer has been reported to stabilize anionic or even neutral intermediates leading to the reduction in charge transfer resistance for higher concentration of KOH (Fig. S14) [60].

3.5. Stability of HFGDEs and performance comparison with other studies

To investigate the long-term stability of the HFGDEs for CORR, CuCube HFGDE was tested in a custom-built flow-cell (Fig. S3). Running the flow-cell reactor, the electrolytes in cathode and anode chambers were circulated (10 ml min^{-1}), and the CO flow rate was kept at 20 ml min^{-1}. KOH at 5 M was used as the electrolyte for long-term test (both catholyte and anolyte) considering the high partial current density of ethylene. Over a period of 36 h at − 0.8 V vs. RHE, the electrode showed stable operation for current density and FE of ethylene as seen in Fig. 4b. Here in the flow-cell a higher current density was obtained compared with the H-cell, and the partial current density of ethylene stayed between 460 and 490 mA cm^{-2}. This is due to more stabilized pH, ion/intermediate concentrations and sufficient CO availability in the vicinity of the electrode due to the catholyte flowing effects [39]. Moreover, the SEM image of the electrode surface after long-term test (Fig. S17) demonstrated the existence of cubic shape Cu particles without any significant changes, therefore the fabricated electrodes can maintain their morphology. XRD pattern of CuCube HFGDE after CORR also showed Cu (100) as the dominant phase (Fig. S18), with a small decrease in Cu (100) intensity, possibly attributed to the slight change in the morphology of the nanocubes during the reaction. Morphological changes in cubic copper under CO_2RR have been reported in the literature [27,61], and it has been shown that changes are related to several factors and can affect the CO_2RR performance. Therefore, we believe that this matter is worth investigating for CORR, since the microenvironment of CO_2RR and CORR are different which can affect the possible dynamic changes in copper cubes. In addition, the ICP-MS analysis showed an increase in the copper concentration of the 5 M KOH electrolyte from 8.9 ppb before CORR to 45.1 after long-term CORR (Table S2), possibly attributed to some slight particle detachment during the reaction. Compared to the post-reaction Cu concentration in KOH electrolyte reported for CO_2RR in the literature [62] (> 300 ppb), we observed a much smaller increase, showing the promising stability of the catalysts here during CORR.

The performance of the CuCube HFGDE in this study is compared with the recent state-of-art studies to produce ethylene as the main product from CORR in Fig. 4c (references can be found in Table S3). The electrodes showed promising performance for current density compared with other conventional planar GDEs, indicating the practicality of hollow fiber electrode configuration for high-rate CORR, which is herein studied for the first time. As mentioned earlier, the employment of HFGDEs for CO_2RR is limited to neutral electrolytes since CO_2 reacts with KOH for flow-through mode in HFGDEs. For the same reason, our previous studies of CO_2RR with HFGEDs in bicarbonate media [20,39,63] could not compete with the planar GDEs (flow-by) in which alkaline electrolytes were used. Herein we conclude that CORR on HFGDEs can outperform the planar GDEs, indicating the promises of this electrode design for gas-phase electrolysis reactions. Future studies can focus on loading the HFGDEs with even more active/selective catalysts for other desired products such as n-propanol/ethanol and developing electrolyte-free HFGDE-based electrolyzers to eliminate the need for liquid electrolytes, which causes mass/electron transfer resistance.

4. Conclusions

In this study, for the first time, hollow fiber GDEs were used for carbon monoxide reduction to C_{2+} products with Cu nanocubes as the active catalyst layer. Compared with the polycrystalline pristine Cu HFGDE, the HFGDE with a nanocube copper layer showed a significantly higher FE for C_{2+} production, with an ethylene FE as high as 68 ± 3%. It was further shown that for the formation C_{2+} products, CORR is superior to CO_2RR both in terms of current density and FE of ethylene as the main product, demonstrating the advantages of CORR over CO_2RR for gas-phase electrolysis in alkaline media. By increasing the concentration of the KOH electrolyte to 5 M, an ethylene partial current density of 460–490 mA cm^{-2} in a flow-cell was achieved at − 0.8 V cs. RHE, which outperforms conventional planar GDEs. Moreover, the HFGDEs were tested in both GDE mode and non-GDE mode (disperssion mode). It was found that the HFGDEs provide a much higher current density and FE of ethylene in the GDE mode. Pushing CO through the hollow fiber porous wall into the electrolyte side likely led to higher local CO concetration, more use of the catalytic active sites of CuCube HFGDE, and the formation of a triple-phase. In contrast, in the dispersion mode, a very high FE of H_2 evolution indicates that electrons are being consumed for water splitting reaction rather than CORR, due to a low CO avaibility caused by the low aqueous solubility of CO and its supply from the bulk electrolyte. This study showcased the potential of the hollow fiber GDE configuration for high-rate gas-phase electrolysis, which may also be considered for other desired products of CORR or other reactions, such as nitrogen reduction to ammonia.

Supporting Information

The schematic of HFGDE preparation, the image of the flow-type reactor, material characterization, and additional CO_2 electrolysis performance can be found in the SI.

CRediT authorship contribution statement

H.R. and L.G. conceived the idea and designed the research. H.R., J. K.H., P.Y., and X.Z. conducted the experiments and characterizations. L. G. conceived the idea and assisted H.R. in the writing and analysis of the data. H.R., J.K.H., and L.G. contributed to the interpretation of the electrochemical data and characterizations. S.S., Z.Z., Z.Y., E.M., and H. W. provided the use of facilities and advised on the experiments and writing. H.R., L.G., S.H., and Z.Y. co-wrote the manuscript. All authors discussed the results and contributed to the revision of the manuscript at

all stages.

Declaration of Competing Interest

The authors declare that they have no known competing financial interests or personal relationships that could have appeared to influence the work reported in this paper.

Data Availability

Data will be made available on request.

Acknowledgements

This study was funded through Laureate Fellowship FL170100086 by the Australian Research Council (ARC), awarded to Professor Zhiguo Yuan and Future Fellowship FT220100166, awarded to Dr Lei Ge. We acknowledge USQ 2022 Capacity Building Grant awarded to Dr Hesamoddin Rabiee. JF and EM acknowledge the financial support for the ARC Centre of Excellence in Synthetic Biology CE200100029. We acknowledge the support from the Center for Microscopy and Microanalysis (CMM) at UQ for SEM, TEM, XRD analyses, and the Environmental Geochemistry Laboratory within the School of Earth and Environmental Sciences at UQ for ICP-MS analysis.

Appendix A. Supporting information

Supplementary data associated with this article can be found in the online version at doi:10.1016/j.apcatb.2023.122589.

References

[1] S. Overa, B.H. Ko, Y. Zhao, F. Jiao, Electrochemical approaches for CO_2 conversion to chemicals: a journey toward practical applications, Acc. Chem. Res. 55 (2022) 638–648.
[2] M.T. Tang, H. Peng, P.S. Lamoureux, M. Bajdich, F. Abild-Pedersen, From electricity to fuels: Descriptors for C1 selectivity in electrochemical CO_2 reduction, Appl. Catal. B 279 (2020) 119384–119394.
[3] Y. Kuang, H. Rabiee, L. Ge, T.E. Rufford, Z. Yuan, J. Bell, H. Wang, High-concentration electrosynthesis of formic acid/formate from CO_2: reactor and electrode design strategies, Energy Environ. Mater. (2023), https://doi.org/10.1002/eem2.12596.
[4] R.M. Arán-Ais, F. Scholten, S. Kunze, R. Rizo, B. Roldan Cuenya, The role of in situ generated morphological motifs and Cu(i) species in C2+ product selectivity during CO_2 pulsed electroreduction, Nat. Energy 5 (2020) 317–325.
[5] A.R. Woldu, Z. Huang, P. Zhao, L. Hu, D. Astruc, Electrochemical CO_2 reduction (CO_2RR) to multi-carbon products over copper-based catalysts, Coord. Chem. Rev. 454 (2022) 214340–214368.
[6] N. Gutiérrez-Guerra, L. Moreno-López, J.C. Serrano-Ruiz, J.L. Valverde, A. de Lucas-Consuegra, Gas phase electrocatalytic conversion of CO 2 to syn-fuels on Cu based catalysts-electrodes, Appl. Catal. B 188 (2016) 272–282.
[7] N.S. Romero Cuellar, K. Wiesner-Fleischer, M. Fleischer, A. Rucki, O. Hinrichsen, Advantages of CO over CO_2 as reactant for electrochemical reduction to ethylene, ethanol and n-propanol on gas diffusion electrodes at high current densities, Electrochim. Acta 307 (2019) 164–175.
[8] M.E. Leonard, L.E. Clarke, A. Forner-Cuenca, S.M. Brown, F.R. Brushett, Investigating electrode flooding in a flowing electrolyte, gas-fed carbon dioxide electrolyzer, ChemSusChem 13 (2020) 400–411.
[9] M. Ma, E.L. Clark, K.T. Therkildsen, S. Dalsgaard, I. Chorkendorff, B. Seger, Insights into the carbon balance for CO_2 electroreduction on Cu using gas diffusion electrode reactor designs, Energy Environ. Sci. 13 (2020) 977–985.
[10] Y.L. Ji, A.X. Guan, G.F. Zheng, Copper-based catalysts for electrochemical carbon monoxide reduction, Cell Rep. Phys. Sci. 3 (2022) 101072–101094.
[11] H. Song, J.T. Song, B. Kim, Y.C. Tan, J. Oh, Activation of C2H4 reaction pathways in electrochemical CO_2 reduction under low CO_2 partial pressure, Appl. Catal. B 272 (2020) 119049–119056.
[12] G.L. De Gregorio, T. Burdyny, A. Loiudice, P. Iyengar, W.A. Smith, R. Buonsanti, Facet-dependent selectivity of Cu catalysts in electrochemical CO_2 reduction at commercially viable current densities, Acs Catal. 10 (2020) 4854–4862.
[13] F.S. Roberts, K.P. Kuhl, A. Nilsson, Electroreduction of carbon monoxide over a copper nanocube catalyst: surface structure and pH dependence on selectivity, ChemCatChem 8 (2016) 1119–1124.
[14] G.O. Larrazabal, V. Okatenko, I. Chorkendorff, R. Buonsanti, B. Seger, Investigation of Ethylene and Propylene Production from CO_2 Reduction over Copper Nanocubes in an MEA-Type Electrolyzer, ACS Appl. Mater. Interfaces 14 (2022) 7779–7787.
[15] H. Rabiee, L. Ge, X. Zhang, S. Hu, M. Li, Z. Yuan, Gas diffusion electrodes (GDEs) for electrochemical reduction of carbon dioxide, carbon monoxide, and dinitrogen to value-added products: a review, Energy Environ. Sci. 14 (2021) 1959–2008.
[16] X.-Q. Li, G.-Y. Duan, J.-W. Chen, L.-J. Han, S.-J. Zhang, B.-H. Xu, Regulating electrochemical CO2RR selectivity at industrial current densities by structuring copper@poly(ionic liquid) interface, Appl. Catal. B 297 (2021) 120471–120483.
[17] L. Ge, H. Rabiee, M. Li, S. Subramanian, Y. Zheng, J.H. Lee, T. Burdyny, H. Wang, Electrochemical CO_2 reduction in membrane-electrode assemblies, Chem 8 (2022) 663–692.
[18] D. Wakerley, S. Lamaison, J. Wicks, A. Clemens, J. Feaster, D. Corral, S.A. Jaffer, A. Sarkar, M. Fontecave, E.B. Duoss, S. Baker, E.H. Sargent, T.F. Jaramillo, C. Hahn, Gas diffusion electrodes, reactor designs and key metrics of low-temperature CO_2 electrolysers, Nat. Energy 7 (2022) 130–143.
[19] M.R. Li, M.N. Idros, Y.M. Wu, S. Garg, S. Gao, R.J. Lin, H. Rabiee, Z.H. Li, L. Ge, T. E. Rufford, Z.H. Zhu, L.Y. Li, G. Wang, Unveiling the effects of dimensionality of tin oxide-derived catalysts on CO_2 reduction by using gas-diffusion electrodes, React. Chem. Eng. 6 (2021) 345–352.
[20] H. Rabiee, X. Zhang, L. Ge, S. Hu, M. Li, S. Smart, Z. Zhu, Z. Yuan, Tuning the Product Selectivity of the Cu Hollow Fiber Gas Diffusion Electrode for Efficient CO_2 Reduction to Formate by Controlled Surface Sn Electrodeposition, ACS Appl. Mater. Interfaces 12 (2020) 21670–21681.
[21] R. Kas, K.K. Hummadi, R. Kortlever, P. de Wit, A. Milbrat, M.W. Luiten-Olieman, N. E. Benes, M.T. Koper, G. Mul, Three-dimensional Porous Hollow Fibre Copper Electrodes for Efficient and High-rate Electrochemical Carbon Dioxide Reduction, Nat. Commun. 7 (2016) 10748–10754.
[22] H. Rabiee, L. Ge, S. Hu, H. Wang, Z. Yuan, Microtubular electrodes: An emerging electrode configuration for electrocatalysis, bioelectrochemical and water treatment applications, Chem. Eng. J. 450 (2022) 138476–138496.
[23] F.P. Garcia de Arquer, C.T. Dinh, A. Ozden, J. Wicks, C. McCallum, A.R. Kirmani, D.H. Nam, C. Gabardo, A. Seifitokaldani, X. Wang, Y.C. Li, F. Li, J. Edwards, L. J. Richter, S.J. Thorpe, D. Sinton, E.H. Sargent, CO_2 electrolysis to multicarbon products at activities greater than 1 A cm(-2), Science 367 (2020) 661–666.
[24] M. Duarte, B. De Mot, J. Hereijgers, T. Breugelmans, Electrochemical Reduction of CO_2: Effect of Convective CO_2 Supply in Gas Diffusion Electrodes, Chemelectrochem 6 (2019) 5596–5602.
[25] H. Rabiee, L. Ge, J. Zhao, X. Zhang, M. Li, S. Hu, S. Smart, T.E. Rufford, Z. Zhu, H. Wang, Z. Yuan, Regulating the reaction zone of electrochemical CO_2 reduction on gas-diffusion electrodes by distinctive hydrophilic-hydrophobic catalyst layers, Appl. Catal. B 310 (2022) 121362–121372.
[26] J.Y. Kim, P. Zhu, F.Y. Chen, Z.Y. Wu, D.A. Cullen, H.T. Wang, Recovering carbon losses in CO_2 electrolysis using a solid electrolyte reactor, Nat. Catal. 5 (2022) 288–299.
[27] P. Grosse, D. Gao, F. Scholten, I. Sinev, H. Mistry, B. Roldan, Cuenya, Dynamic Changes in the Structure, Chemical State and Catalytic Selectivity of Cu Nanocubes during CO_2 Electroreduction: Size and Support Effects, Angew. Chem. 57 (2018) 6192–6197.
[28] T. Moller, F. Scholten, T.N. Thanh, I. Sinev, J. Timoshenko, X. Wang, Z. Jovanov, M. Gliech, B. Roldan Cuenya, A.S. Varela, P. Strasser, Electrocatalytic CO_2 Reduction on CuOx Nanocubes: Tracking the Evolution of Chemical State, Geometric Structure, and Catalytic Selectivity using Operando Spectroscopy, Angew. Chem. 59 (2020) 17974–17983.
[29] D. Gao, I. Zegkinoglou, N.J. Divins, F. Scholten, I. Sinev, P. Grosse, B. Roldan Cuenya, Plasma-Activated Copper Nanocube Catalysts for Efficient Carbon Dioxide Electroreduction to Hydrocarbons and Alcohols, ACS Nano 11 (2017) 4825–4831.
[30] F.S. Roberts, K.P. Kuhl, A. Nilsson, High Selectivity for Ethylene from Carbon Dioxide Reduction over Copper Nanocube Electrocatalysts, Angew. Chem. 127 (2015) 5268–5271.
[31] J. Li, X. Chang, H. Zhang, A.S. Malkani, M.J. Cheng, B. Xu, Q. Lu, Electrokinetic and in situ spectroscopic investigations of CO electrochemical reduction on copper, Nat. Commun. 12 (2021) 3264.
[32] K.J. Schouten, Z. Qin, E. Perez Gallent, M.T. Koper, Two pathways for the formation of ethylene in CO reduction on single-crystal copper electrodes, J. Am. Chem. Soc. 134 (2012) 9864–9867.
[33] K.J.P. Schouten, E. Pérez Gallent, M.T.M. Koper, The influence of pH on the reduction of CO and CO_2 to hydrocarbons on copper electrodes, J. Electroanal. Chem. 716 (2014) 53–57.
[34] A.A. Peterson, F. Abild-Pedersen, F. Studt, J. Rossmeisl, J.K. Norskov, How copper catalyzes the electroreduction of carbon dioxide into hydrocarbon fuels, Energy Environ. Sci. 3 (2010) 1311–1315.
[35] W.J. Durand, A.A. Peterson, F. Studt, F. Abild-Pedersen, J.K. Nørskov, Structure effects on the energetics of the electrochemical reduction of CO_2 by copper surfaces, Surf. Sci. 605 (2011) 1354–1359.
[36] J.H. Montoya, C. Shi, K. Chan, J.K. Norskov, Theoretical Insights into a CO Dimerization Mechanism in CO_2 Electroreduction, J. Phys. Chem. Lett. 6 (2015) 2032–2037.
[37] D. Ren, N.T. Wong, A.D. Handoko, Y. Huang, B.S. Yeo, Mechanistic Insights into the Enhanced Activity and Stability of Agglomerated Cu Nanocrystals for the Electrochemical Reduction of Carbon Dioxide to n-Propanol, J. Phys. Chem. Lett. 7 (2016) 20–24.
[38] Y. Hori, R. Takahashi, Y. Yoshinami, A. Murata, Electrochemical reduction of CO at a copper electrode, J. Phys. Chem. B 101 (1997) 7075–7081.
[39] H. Rabiee, L. Ge, X. Zhang, S. Hu, M. Li, S. Smart, Z. Zhu, H. Wang, Z. Yuan, Stand-alone asymmetric hollow fiber gas-diffusion electrodes with distinguished bronze phases for high-efficiency CO_2 electrochemical reduction, Appl. Catal. B 298 (2021) 120538–120548.

[40] H. Xiang, S. Rasul, K. Scott, J. Portoles, P. Cumpson, E.H. Yu, Enhanced selectivity of carbonaceous products from electrochemical reduction of CO_2 in aqueous media, J. CO_2 Util. 30 (2019) 214–221.
[41] Y.J. Pang, J. Li, Z.Y. Wang, C.S. Tang, P.L. Hsieh, T.T. Zhuang, Z.Q. Liang, C. Q. Zou, X. Wang, P. De Luna, J.P. Edwards, Y. Xu, F.W. Li, C.T. Dinh, M. Zhong, Y. H. Lou, D. Wu, L.J. Chen, E.H. Sargent, D. Sinton, Efficient electrocatalytic conversion of carbon monoxide to propanol using fragmented copper, Nat. Catal. 2 (2019) 251–258.
[42] J.M. Strain, S. Gulati, S. Pishgar, J.M. Spurgeon, Pulsed Electrochemical Carbon Monoxide Reduction on Oxide-Derived Copper Catalyst, ChemSusChem 13 (2020) 3028–3033.
[43] J. Li, Z. Wang, C. McCallum, Y. Xu, F. Li, Y. Wang, C.M. Gabardo, C.-T. Dinh, T.-T. Zhuang, L. Wang, J.Y. Howe, Y. Ren, E.H. Sargent, D. Sinton, Constraining CO coverage on copper promotes high-efficiency ethylene electroproduction, Nat. Catal. 2 (2019) 1124–1131.
[44] M. Jouny, W. Luc, F. Jiao, High-rate electroreduction of carbon monoxide to multi-carbon products, Nat. Catal. 1 (2018) 748–755.
[45] L. Wang, S. Nitopi, A.B. Wong, J.L. Snider, A.C. Nielander, C.G. Morales-Guio, M. Orazov, D.C. Higgins, C. Hahn, T.F. Jaramillo, Electrochemically converting carbon monoxide to liquid fuels by directing selectivity with electrode surface area, Nat. Catal. 2 (2019) 702–708.
[46] L. de Sousa, N.E. Benes, G. Mul, Evaluating the Effects of Membranes, Cell Designs, and Flow Configurations on the Performance of Cu-GDEs in Converting CO_2 to CO, ACS EST Engi. 2 (2022) 2034–2042.
[47] S. Li, W. Chen, X. Dong, C. Zhu, A. Chen, Y. Song, G. Li, W. Wei, Y. Sun, Hierarchical micro/nanostructured silver hollow fiber boosts electroreduction of carbon dioxide, Nat. Commun. 13 (2022) 3080.
[48] J. Li, G.X. Chen, Y.Y. Zhu, Z. Liang, A. Pei, C.L. Wu, H.X. Wang, H.R. Lee, K. Liu, S. Chu, Y. Cui, Efficient electrocatalytic CO_2 reduction on a three-phase interface, Nat. Catal. 1 (2018) 592–600.
[49] W. Luc, X. Fu, J. Shi, J.-J. Lv, M. Jouny, B.H. Ko, Y. Xu, Q. Tu, X. Hu, J. Wu, Q. Yue, Y. Liu, F. Jiao, Y. Kang, Two-dimensional copper nanosheets for electrochemical reduction of carbon monoxide to acetate, Nat. Catal. 2 (2019) 423–430.
[50] M. Dunwell, W. Luc, Y. Yan, F. Jiao, B. Xu, Understanding Surface-Mediated Electrochemical Reactions: CO_2 Reduction and Beyond, ACS Catal. 8 (2018) 8121–8129.
[51] H.P. Duong, N.-H. Tran, G. Rousse, S. Zanna, M.W. Schreiber, M. Fontecave, Highly Selective Copper-Based Catalysts for Electrochemical Conversion of Carbon Monoxide to Ethylene Using a Gas-Fed Flow Electrolyzer, ACS Catal. 12 (2022) 10285–10293.
[52] M. Ma, W. Deng, A. Xu, D. Hochfilzer, Y. Qiao, K. Chan, I. Chorkendorff, B. Seger, Local reaction environment for selective electroreduction of carbon monoxide, Energy Environ. Sci. 15 (2022) 2470–2478.
[53] A.S. Varela, M. Kroschel, T. Reier, P. Strasser, Controlling the selectivity of CO_2 electroreduction on copper: The effect of the electrolyte concentration and the importance of the local pH, Catal. Today 260 (2016) 8–13.
[54] L. Yao, Y. Pan, X. Shen, D. Wu, A. Bentalib, Z. Peng, Utilizing hydrogen underpotential deposition in CO reduction for highly selective formaldehyde production under ambient conditions, Green. Chem. 22 (2020) 5639–5647.
[55] G. Marcandalli, A. Goyal, M.T.M. Koper, Electrolyte Effects on the Faradaic Efficiency of CO_2 Reduction to CO on a Gold Electrode, Acs Catal. 11 (2021) 4936–4945.
[56] L. Peng, Y. Wang, Y. Wang, N. Xu, W. Lou, P. Liu, D. Cai, H. Huang, J. Qiao, Separated growth of Bi-Cu bimetallic electrocatalysts on defective copper foam for highly converting CO_2 to formate with alkaline anion-exchange membrane beyond KHCO3 electrolyte, Appl. Catal. B 288 (2021) 120003–120011.
[57] H. Xiao, T. Cheng, W.A. Goddard 3rd, R. Sundararaman, Mechanistic Explanation of the pH Dependence and Onset Potentials for Hydrocarbon Products from Electrochemical Reduction of CO on Cu (111), J. Am. Chem. Soc. 138 (2016) 483–486.
[58] J. Andraos, A.J. Kresge, Correlation of rates of uncatalyzed and hydroxide-ion catalyzed ketene hydration. A mechanistic application and solvent isotope effects on the uncatalyzed reaction, Can. J. Chem. 78 (2000) 508–515.
[59] A. Goyal, M.T.M. Koper, Understanding the role of mass transport in tuning the hydrogen evolution kinetics on gold in alkaline media, J. Chem. Phys. 155 (2021), 134705.
[60] S. Verma, X. Lu, S. Ma, R.I. Masel, P.J. Kenis, The effect of electrolyte composition on the electroreduction of CO_2 to CO on Ag based gas diffusion electrodes, Phys. Chem. Chem. Phys. 18 (2016) 7075–7084.
[61] P. Grosse, A. Yoon, C. Rettenmaier, A. Herzog, S.W. Chee, B. Roldan Cuenya, Dynamic transformation of cubic copper catalysts during CO(2) electroreduction and its impact on catalytic selectivity, Nat. Commun. 12 (2021) 6736.
[62] X. Zhang, J. Li, Y.Y. Li, Y. Jung, Y. Kuang, G. Zhu, Y. Liang, H. Dai, Selective and High Current CO_2 Electro-Reduction to Multicarbon Products in Near-Neutral KCl Electrolytes, J. Am. Chem. Soc. 143 (2021) 3245–3255.
[63] H. Rabiee, L. Ge, X. Zhang, S. Hu, M. Li, S. Smart, Z. Zhu, Z. Yuan, Shape-tuned electrodeposition of bismuth-based nanosheets on flow-through hollow fiber gas diffusion electrode for high-efficiency CO_2 reduction to formate, Appl. Catal. B 286 (2021) 119945–119956.